Corrosion Science 154 (2019) 61–69

Contents lists available at ScienceDirect

Corrosion Science

journal homepage: www.elsevier.com/locate/corsci

The effect of surface vacancies on the interactions of Cl with a α-Fe_2O_3 (0001) surface and the role of Cl in depassivation

Qin Pang[a], Hossein DorMohammadi[b], O. Burkan Isgor[b], Líney Árnadóttir[a,*]

[a] School of Chemical, Biological and Environmental Engineering, Oregon State University, Corvallis, OR, 97331, United States
[b] School of Civil and Construction Engineering, Oregon State University, Corvallis, OR, 97331, United States

ARTICLE INFO

Keywords:
Iron passive film
Cl-induced depassivation
Hematite
Vacancy
DFT + U
Ion exchange model
Point defect model

ABSTRACT

This study provides molecular insights into the initial stages of Cl-induced depassivation of iron passive film by studying the interactions of Cl with pristine and vacancy surfaces of α-Fe_2O_3 (0001). Subsurface Cl is found to be less stable than adsorbed Cl which contradicts the ion exchange model that postulates Cl ingress into the passive film. Comparison of vacancy formation energy shows that Cl can enhance the surface Fe vacancy formation, which is consistent with the point defect model. Additionally, the energy difference of vacancies in different oxide layers supports the diffusion direction proposed by the point defect model.

1. Introduction

Corrosion of carbon steel inside reinforced concrete is a major challenge for modern infrastructure. In alkaline environments, such as those observed inside concrete (pH > 13), passive film is formed on the surface of carbon steel (or iron), which protects the surface from active corrosion. The passive film has been proposed to be composed of two layers: an outer layer which contains Fe^{III}-rich oxides/oxyhydroxides and an inner layer which consists of Fe^{II}-rich oxides/oxyhydroxides [1–3]. A transition zone has also been observed between the two layers. The exact structure of the film is complex but hematite (α-Fe_2O_3) is considered to be one of the dominant structures of the outer layer [3].

Experimental studies have shown that Cl can cause depassivation of the passive film in highly alkaline electrolytes [1–5], but the mechanism of this Cl-induced depassivation is still under debate. There are several proposed mechanisms to explain the Cl-induced depassivation process [6–10]. Here two of the commonly proposed mechanisms will be investigated and compared: the ion exchange model [6,8] and the point defect model [7–10]. Both models propose that the Cl-induced depassivation starts with the adsorption of Cl on the film surface. In the ion exchange model, Cl is proposed to penetrate into the bulk of the passive film by occupying O vacancies or exchanging with the bulk O. With the Cl in the passive film, the passive film breaks down, causing depassivation. The penetration of Cl is the key step in the ion exchange model. In the point defect model, the role of Cl in the depassivation process is to catalyze Fe vacancy formation on the surface. It also describes the possibility of Cl occupying the surface O vacancies, which then contributes to the formation of surface Fe vacancy. The Fe vacancies are proposed to diffuse from the oxide/solution interface to the oxide/metal interface while O vacancies diffuse in an opposite direction. Eventually, the Fe vacancy concentration at the oxide/metal interface increases and the vacancies can combine, forming voids which lead to breakdown of the passive film.

The Cl-induced depassivation of other metal passive films, such as Ni and Al, have been studied using density functional theory (DFT) [11–13]. For example, a DFT study of Cl interactions with NiO (111) surface [11] found that Cl penetration into the subsurface is favorable at high Cl coverage (> 70%), but the resulting reconstructed structure is not supported by experimental findings. Also, the simulations did not show adsorption-induced thinning of the oxide nor Cl penetration from the undefective terrace of the Ni passive film as hypothesized by experimental studies [14,15]. Another study of Cl interactions with a stepped NiO (553) surface [12] showed signs of the Cl-induced dissolution of the step edge and suggested local penetration of Cl atoms into the oxide lattice. A study of the Cl adsorption on a α-Al_2O_3 (0001) surface showed that at low Cl coverage the Cl interactions have little effect on the surface structure [13], which suggests that the Cl adsorption would not lead to surface breakdown.

In this study we use an α-Fe_2O_3 (0001) surface, a predominate facet of α-Fe_2O_3 [16], as a model Fe^{III} oxide surface to study the role of Cl in Cl-induced depassivation. The Fe-termination has been proposed to be

* Corresponding author.
E-mail address: liney.arnadottir@oregonstate.edu (L. Árnadóttir).

https://doi.org/10.1016/j.corsci.2019.03.052
Received 27 October 2018; Received in revised form 16 February 2019; Accepted 31 March 2019
Available online 03 April 2019
0010-938X/

the most stable termination of α-Fe_2O_3 (0001) in a vacuum by DFT calculations [17,18], and the same termination has been observed in aqueous environment using Scanning Tunneling Microscopy (STM) [19]. Our previous study [20] of the adsorption of Cl and OH on the pristine surface of α-Fe_2O_3 (0001) suggests that Cl and OH adsorption follow a similar trend with OH being slightly more stable (by 0.08 eV) at low coverage. The effect of the two adsorbates on the surface structure is small, pulling the nearest Fe atom out of the surface by only ˜0.6 Å at higher coverage. This indicates that the adsorption of Cl and OH on the pristine surface alone is unlikely to induce the breakdown of the oxide or the ingress of Cl into the film. In this study we focus on the role of Cl in the depassivation of iron oxide surface and the role of surface vacancies. Computational studies of point defective α-Fe_2O_3 (0001) surface, with Fe- and O surface vacancies, showed that Fe- and O vacancies are stable on the α-Fe_2O_3 surface at certain oxygen chemical potential. The vacancies change the local surface geometry and affect both the electronic and magnetic properties of the surface [18,21–23]. Here we study the interactions of Cl with pristine Fe-terminated α-Fe_2O_3 (0001) surface as well as vacancy surfaces to gain molecular insights into the depassivation mechanism and compare our findings with two current depassivation models, the ion exchange model and the point defect model, to explore the feasibility of these models in explaining the depassivation process.

2. Computational methods and surface models

2.1. Computational methods

All calculations were performed using spin-polarized Density Functional Theory (DFT) [24,25] as employed in Vienna Ab initio Simulation Package (VASP) [26–29]. The projector augmented wave potential (PAW) [30] and plane wave basis set were used for all calculations. The generalized gradient approximation (GGA) of the Perdew-Burke-Ernzerhof (PBE) functional [31,32] was used to describe the exchange-correlation potential. In order to correct the on-site Coulomb interactions of Fe 3d electrons, the DFT + U [33–37] method introduced by Dudarev et al. [38] was applied with U = 4 eV based on a previous study [20]. The cutoff energy was 400 eV for all calculations. A k-point grid with a 3 × 3 × 1 Monkhorst-Pack [39] mesh was used for surface relaxation and calculation of total energies. For calculation of the electronic density of states (DOS) for the surface slab, a 7 × 7 × 1 grid and tetrahedron-smearing method with Blöchl correction were used. All calculations were considered converged when the force reached below 0.02 eV/Å. Bader charge analysis was performed to obtain the atomic charges for the clean surfaces (0 ML Cl coverage) and selected adsorption systems using the method developed by Henkelman et al. [40–43] The climbing image nudged elastic band (CI-NEB) method [44] was used to calculate the diffusion barriers of Fe and O vacancies toward the bulk or toward the vacuum, respectively.

2.2. Surface models

The unit cell of α-Fe_2O_3 contains 30 atoms following a -Fe-O3-Fe- periodicity along the [0001] direction. The optimized lattice constants for the unit cell were a = b = 5.027 Å and c = 13.724 Å (c/a = 2.73), and in good agreement with experiments (a = b = 5.035 Å and c = 13.747 Å) [45]. The Fe-terminated (0001) surface was modeled by applying a 15 Å vacuum space between the periodic slabs in z direction. The modeled supercells have 2 unit cells in the x and y directions, and one unit cell in z direction, as shown in Fig. 1, containing approximately 120 atoms depending on the number of vacancies. For all surface calculations, the top 8 atomic layers were relaxed, with the bottom 10 atomic layers fixed. The number of relaxed layers is determined by converging the structural changes and the change in total energy with respect to the relaxed layers. The energy change is very small beyond 6 relaxed layers (< 0.01 eV/atom). Four different surfaces are included in this study: pristine surface, Fe vacancy surface, O vacancy surface, and Fe-O pair vacancy surface. Top views of the four surfaces and a side view of the pristine surface are shown in Fig. 1. Vacancies were created by removing an Fe or an O atom from the pristine surface keeping a low surface vacancy concentration of 0, 6.25%, 6.25% and 12.5% respectively for the four surfaces. The Fe-O pair vacancy surface is included to investigate the effect of high local concentration of vacancies. The overall charge of each system is neutral and the magnetic state is antiferromagnetic (+ + - -) based on our previous study [20]. The adsorption sites on the four surfaces are shown in Fig. 1. Fe1 is the outermost Fe site on all surfaces, while Fe2 is the outermost Fe site closest to the O vacancy which only exist on the O vacancy surface. V_{Fe} and V_O refer to the Fe- and O vacancy sites, respectively.

2.3. Definition of energies

The adsorption energy is calculated to investigate the strength of the Cl-surface interactions. The adsorption energy per adsorbate (E_{ads}) is defined as:

$$E_{ads} = (E_{slab+n\times Cl} - (E_{slab} + n \times E_{Cl}))/n \quad (1)$$

where $E_{slab+n\times Cl}$ is the total energy of the surface slab and n Cl on the surface, E_{slab} and E_{Cl} are the energy of clean surface slab and the isolated adsorbate (Cl) in the vacuum, respectively. The number of Cl on the surface, n, can be 1–4 corresponding to the Cl coverage of 1/12 ML to 4/12 ML. The adsorption energy is normalized by the number of adsorbate(s) (n) to get the adsorption energy per adsorbate.

To study the thermodynamic stability of subsurface Cl, we define an insertion energy, E_{ins}, similar to the insertion of Cl studied by Bouzoubaa et al. [11], using Eq. (2).

$$E_{ins} = E_{Cl/subx} - E_{ref} \quad (2)$$

where $E_{Cl/subx}$ represents the total energy of the configuration with one Cl in the subsurface, which is either the second layer ($x = 2$) or fifth layer ($x = 5$). E_{ref} is the total energy of Cl adsorbed on the surface ($E_{slab+n\times Cl}$) for second-layer insertion or the energy of Cl in the second layer $E_{Cl/sub2}$ for fifth-layer insertion. A positive value indicates that the subsurface Cl is less stable than the adsorbed Cl.

The vacancy formation energy is calculated for the clean surfaces to study the stability of surface vacancies and for the surfaces with adsorbed Cl to study the effect of Cl on the vacancy formation. The vacancy formation energy is defined as follows:

$$E_{form} = (E_{ref-atom(s)} + E_{atom(s)}) - E_{ref} \quad (3)$$

where ($E_{ref\text{-}atom(s)} + E_{atom(s)}$) is the combined energy of the surface with the vacancy ($E_{ref\text{-}atom(s)}$) and the atom(s) removed to make the vacancy, at an infinite distance. The energy of the reference surface with the atom(s) still on the surface is represented using E_{ref}. For the formation of all O vacancies, only an O atom is removed to create the vacancy and $E_{atom(s)}$ is the energy of isolated O in the vacuum. For clean surface (0 ML Cl coverage), only an Fe atom is removed to form an Fe vacancy and $E_{atom(s)}$ is the energy of isolated Fe in the vacuum. At higher Cl coverages, Cl adsorbs on Fe and/or occupies O vacancies, the removed species are $FeCl_y$ (y = 1 for pristine surface and y = 2 for O vacancy surface). A positive value of E_{form} suggests an endothermic vacancy formation. A graphical illustration of the definition of vacancy formation energy can be found in the supplementary information.

To determine the most favorable vacancy diffusion direction, the relative stability of the vacancy in the bulk and on the surface is determined using Eq. (4).

$$E_{\Delta v} = E_{n\times Cl+slab(va/bulk)} - E_{n\times Cl+slab(va/surf)} \quad (4)$$

where $E_{n\times Cl+slab(va/bulk)}$ is the energy of the slab with an Fe vacancy in the sixth layer or O vacancy in the fifth layer at the Cl coverage where n is 0 to 4 corresponding to 0 (clean surface) to 4/12 ML Cl coverage. $E_{n\times Cl+slab(va/surf)}$ is the energy of the system where the same kind of

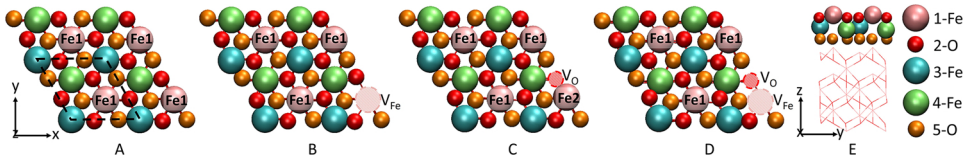

Fig. 1. Top view of the simulation cell for the four Fe-terminated α-Fe_2O_3 (0001) surfaces and side view of the pristine surface. **(A)** Pristine surface. A single unit cell is shown by a dashed rhombus, and the simulation cell is four unit cells. **(B)** Fe vacancy surface. **(C)** O vacancy surface. **(D)** Fe-O pair vacancy surface. **(E)** Side view of the pristine surface. The top 5 atomic layers are shown with spheres. Pink, cyan and lime atoms are Fe atoms in first, third and fourth layers, respectively. Red and orange atoms are O atoms in second and fifth layers, respectively. The Fe- and O vacancy sites are shown in pink and red dashed circles and labeled with V_{Fe} or V_O respectively. This color scheme is used throughout this paper unless otherwise specified. The bottom layers are shown with lines for clarity. Fe1 and Fe2 are the atop sites of the outermost Fe, and V_{Fe} and V_O are the vacancy sites.

vacancy is on the surface. A positive $E_{\Delta v}$ value would indicate that the vacancy is energetically more favorable to be closer to or on the surface and a negative value would suggest that the vacancy is more stable in the bulk of the oxide.

3. Results and discussion

Cl-induced depassivation has been proposed to proceed through several different mechanisms [8]. Here we focus on two of them; the ion exchange model, where Cl ions enhance depassivation through penetration into the bulk oxygen lattice [6], and the point defect model, where Cl ions enhance the surface Fe vacancy formation thus increase the concentration of Fe vacancy in the bulk due to the diffusion of the vacancies [7]. A key difference between these two models is the location of the chloride: in the ion exchange model the Cl is assumed to be subsurface while in the point defect model the Cl catalyzes the surface Fe vacancy formation. To gain a molecular insight into these processes and the initial stages of Cl-induced depassivation, we studied the surface properties and Cl interactions with Fe-terminated α-Fe_2O_3 (0001) surfaces including pristine surface and three vacancy surfaces.

3.1. Surface properties of vacancy surfaces

The properties of vacancy surfaces are studied and compared with the pristine surface. The surface properties studied here are the surface relaxation, vacancy formation energy, electronic properties and magnetic properties.

3.1.1. Surface relaxation and vacancy formation energy

All vacancy surfaces show some relaxation caused by the vacancies, but the effects are localized. The structural changes caused by Fe vacancy are smaller than changes caused by the O vacancy and are distributed among the three closest O atoms, which move toward the bulk by about 0.13 Å. Formation of an O vacancy affects mostly the outermost Fe atom closest to the vacancy which shifts toward the bulk by about 0.5 Å. Similarly, the nearest Fe relaxes about 0.7 Å toward the bulk while the oxygen atoms move toward the bulk by 0.13 Å on the Fe-O pair vacancy surface. The relaxation of the O- and Fe-O pair vacancy surfaces lead to slightly different surface structures where the previously second layer O atoms are now on the surface. More details of this surface relaxation are given as supplementary information.

The formation energies (Eq. (3)) for Fe- and O vacancies relative to clean pristine surface are listed in Table 1. The vacancy formation is endothermic for all surface vacancies, and the formation of an Fe vacancy is more endothermic than the formation of O vacancy, in qualitative agreement with previous studies [21,23]. The energy required to create an Fe-O pair vacancy (11.38 eV) is less than the combined formation energy of a single Fe vacancy (8.10 eV) and a single O vacancy (6.24 eV) by about 3 eV, suggesting a slight stabilization effect for the pair vacancy. The reason for this difference lies in the smaller number of Fe-O bonds broken when forming the pair vacancy. Creating two single Fe- and O vacancy breaks total of 6 Fe-O bonds (3 and 3 respectively), which is 1 Fe-O bond more than creating Fe-O pair vacancy. This stabilization effect indicates that vacancy formation energies would be lower on less ideal surfaces which would have more defects and vacancies.

Table 1
Vacancy formation energy relative to clean pristine surface. The formation energies from previous DFT studies are listed for comparison.

Surface type	Vacancy type	Vacancy formation energy (eV)	
Fe vacancy surface	Fe vacancy	8.10	7.71[a], 7.92[b]
O vacancy surface	O vacancy	6.24	5.51[a]
Fe-O pair vacancy surface	Fe- and O vacancy	11.38	

[a,b] Comparison with previous studies of (a) Ling et al. [21] and (b) by Yin et al. [23].

3.1.2. Electronic properties

Changes in the electronic properties of the surfaces are investigated using Bader charge analysis [40–43] (Fig. 2) and through calculations of the density of states (DOS) (Fig. 3). This analysis provides further insights into the effect of vacancies on the electronic structure of the surfaces and adsorbate interactions with the different surfaces.

In the bulk, the Bader charge for Fe and O is around +1.73 e (losing electrons) and −1.15 e (gaining electrons) (ratio +3/-2), respectively, suggesting that the Fe atoms are Fe^{III} [46,47]. The surface atoms (pink and red) generally have slightly smaller charge, around +1.60 e and -1.10 e (ratio +2.91/−2) for Fe and O, respectively (Fig. 2). The absolute charge difference is even smaller for atoms next to a vacancy, which is consistent with the lower coordination of these atoms. Fig. 2 shows the Bader charge of the top 4 layers for the four surfaces. For the Fe vacancy surface (Fig. 2B) the charge on the three nearest oxygen atoms increases by 0.3 e (gaining less charge) relative to the pristine surface (Fig. 2A). The three oxygen atoms are also shifted slightly toward the bulk to compensate for the less charge transfer. On the O vacancy surface (Fig. 2C), the Fe atoms closest to the O vacancy show the largest change in charge compared to the pristine surface. The charge of the outermost Fe closest to the O vacancy decreases by 0.4 e relative to the pristine surface leading to +1.18 e Bader charge, which is the lowest Fe charge of any of the four surfaces. This lower charge (+1.18 e) indicates that the Fe atom is closer to Fe^{II} than Fe^{III} which is important when considering Cl interactions with the surface. The charge also decreases on the two other nearest Fe atoms, but the change is smaller, 0.35 e and 0.17 e. The pair vacancy (Fig. 2D) shows similar trend as the individual vacancies but the effects are smaller.

The DOS (Fig. 3) is used to show changes in the density of states for the different α-Fe_2O_3 surfaces. The DOS of the four surfaces is calculated using the entire slabs. The occupied states near the Fermi level are made of mainly O 2p states with small amount of Fe 3d states while the conduction band is made of mostly Fe 3d states, which are consistent with experimental findings [48–50]. The presence of surface and defect states within the band gap for the pristine surface and vacancy surfaces is consistent with the previous studies [22,51,52].

3.1.3. Magnetic properties

The magnetic moment of the Fe atoms near the surface is calculated to investigate the effect of vacancies on the magnetic properties (Fig. 4).

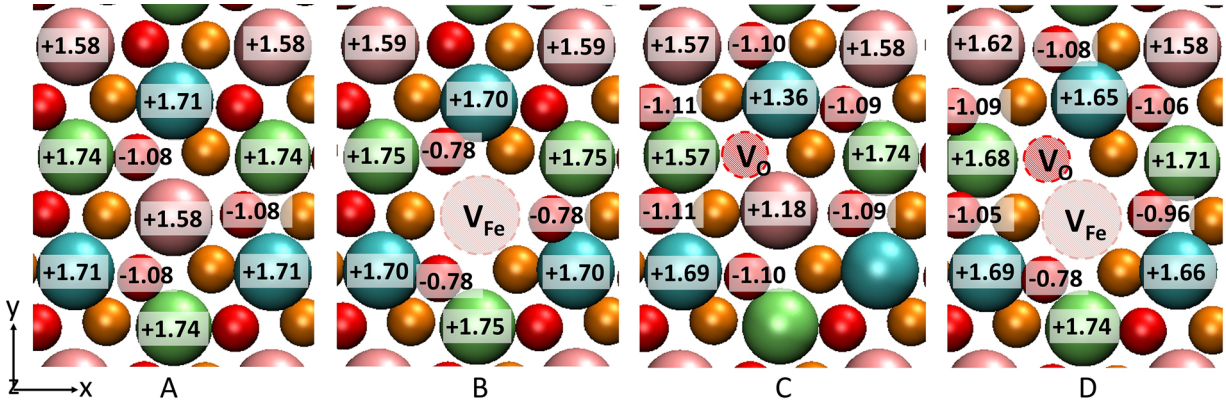

Fig. 2. The Bader charge analysis for the different surfaces. **(A)** Pristine surface. **(B)** Fe vacancy surface. **(C)** O vacancy surface. **(D)** Fe-O pair vacancy surface. Positive value means losing electrons compared to the neutral atom and negative value means gaining electrons compared to the neutral atom.

The positive and negative signs indicate the spin orientation of the magnetic moments (positive indicating up, and negative indicating down orientations).

The calculated magnetic moment for Fe in the α-Fe_2O_3 bulk is 4.15 μ_B, which is about 15% less than the experimental value of 4.9 μ_B [53]. The outermost Fe atoms (Fig. 4A - pink) on the pristine surface have about 0.16 μ_B lower magnetic moment than in the bulk but other surface Fe atoms (cyan and lime) show only minor changes. Formation of both Fe- and O vacancies further decreases the magnetic moments of the nearby Fe atoms (Fig. 4B&C); and Fe vacancy has larger effect than O vacancy. The Fe-O pair vacancy (Fig. 4D) decreases the magnetic moment of the nearby Fe atoms, but the effect is smaller than the individual vacancy.

3.2. Adsorption of Cl on different surfaces

The Cl interactions with α-Fe_2O_3 surface start with Cl adsorption on the surface. The adsorption of Cl on the four surfaces at different coverage was studied to investigate the effect of surface vacancies and Cl coverage on the Cl-surface interactions. We previously showed [20] that on Fe terminated α-Fe_2O_3 (0001) surface Cl is most stable on a top site of the outermost Fe; therefore, here we focus on the Fe top sites and the vacancy sites. The adsorption energy is calculated using Eq. (1), and the results are summarized in Fig. 5. The site labels are the same as before and are shown in Fig. 1.

The adsorption energy of Cl increases with coverage on all surfaces indicating a repulsive interaction (less than 0.11 eV) between the adsorbed Cl. Chloride binds most strongly on the outermost Fe sites, which is the Fe2 site on the O vacancy surface but the Fe1 sites on the other three surfaces. The Cl adsorbs most strongly on the O vacancy surface followed by the Fe-O pair vacancy surface and the pristine surface but the adsorption is weakest on the Fe vacancy surface, suggesting that Cl is stabilized by the O vacancy but destabilized by the Fe vacancy. This correlates well with the Bader charge analysis (Fig. 2)

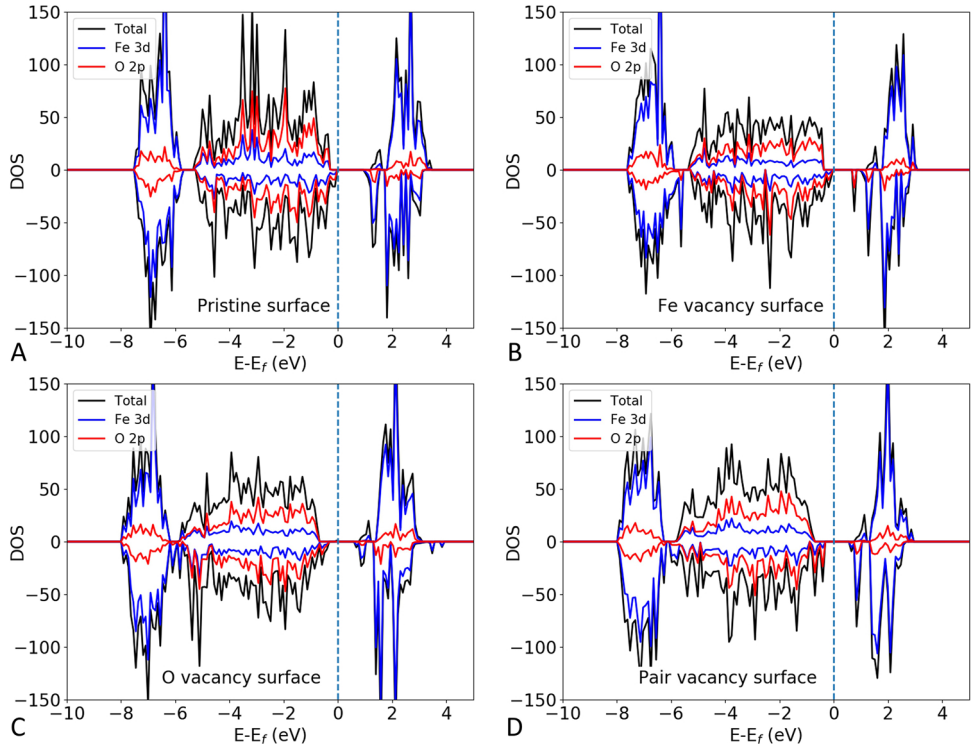

Fig. 3. Density of states (DOS) for clean surfaces. **(A)** Pristine surface. **(B)** Fe vacancy surface. **(C)** O vacancy surface. **(D)** Fe-O pair vacancy surface. The black lines show the total density of states for each surface slab. Blue and red lines show the density of states for all Fe 3d and O 2p states respectively.

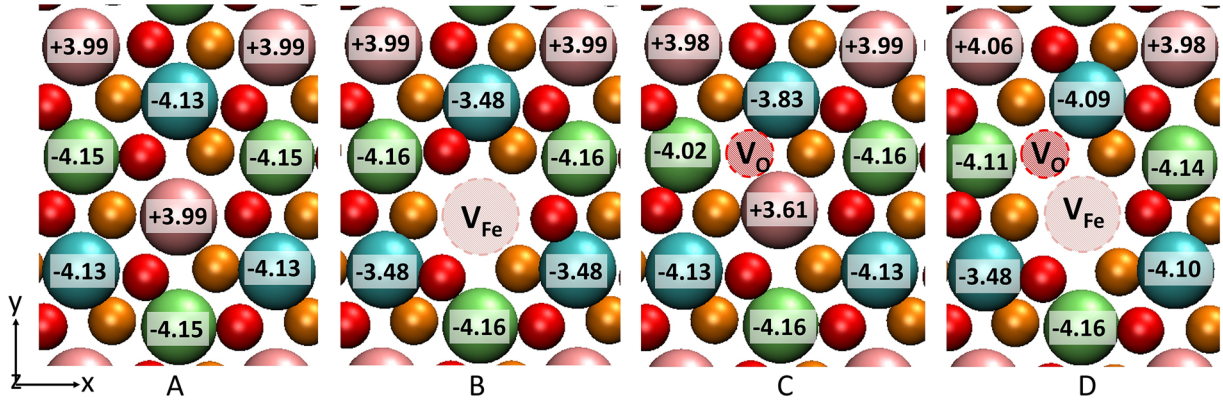

Fig. 4. The magnetic moments (μ_B) of the Fe atoms near the surface. **(A)** Pristine surface. **(B)** Fe vacancy surface. **(C)** O vacancy surface. **(D)** Fe-O pair vacancy surface. Positive and negative sign indicates the up and down orientations of the magnetic moment respectively.

which shows that O- and Fe vacancy decrease the charge transfer from and to the surrounding Fe and O atoms respectively. The Fe-O pair vacancy comprises the effects by making the change in charge transfer smaller than the two individual vacancies.

The oxidation state of the Fe1 sites are the same (Fe^{III}) on the four surfaces, however, the charge of the Fe2 site on the O vacancy surface is 0.4 e lower or +1.18 e which resembles an Fe^{II}. Upon the Cl adsorption, the charge of the Fe atoms (Fe1 sites) below the Cl showed only minor change (+0.02 e), which indicates that these Fe atoms remain as Fe^{III}. While the adsorption of Cl on the Fe2 site caused the charge of the Fe atom below to increase to +1.58 e, indicating an oxidation state change from Fe^{II} to Fe^{III}. More details on the Bader charge analysis can be found in supplementary information. The higher charge transfer is also consistent with a stronger adsorption on the Fe2 site. The stronger interaction of Cl with Fe^{II} surface atoms and the change in oxidation states upon adsorption is in good agreement with the experimental observation that Fe^{II}/Fe^{III} ratio decreases during Cl-induced depassivation [1,2].

Adsorption of Cl has little effect on the surface structure. On the Fe vacancy surface and the pristine surface, the Fe is pulled out by about 0.4 Å. On the O- and Fe-O pair vacancy surfaces, the Fe is pulled out by about 0.5 Å (not including the strong relaxation of the Fe atoms on the clean surfaces), with the resulting Fe-O bond length still at least 0.01 Å shorter than the average Fe-O bond in the bulk.

3.3. Cl insertion into subsurface

To investigate the viability of the ion exchange model in explaining Cl-induced depassivation, Cl ingress into the oxide layer is studied. Specifically, we calculate the insertion energy (Eq. (2)) which represents the relative stability of subsurface Cl in the second layer relative to the surface or between the second and fifth layer, and the results are summarized in Fig. 6. Only one Cl is placed in the bulk for all insertion configurations and the subsurface Cl occupies an O vacancy or exchanges with a bulk O. The bulk O is then adsorbed on the Fe1 surface site to maintain the system size. The coverage here is the surface coverage of Cl so 2/12 ML refers to one Cl in the bulk and two Cl adsorbates on the surface in the calculation cell.

The insertion of Cl into the subsurface is endothermic on all surfaces, but with lower insertion energy for the vacancy surfaces by at least 0.5 eV, suggesting that the vacancies increase the stability of subsurface Cl. The insertion energy into the second subsurface layer

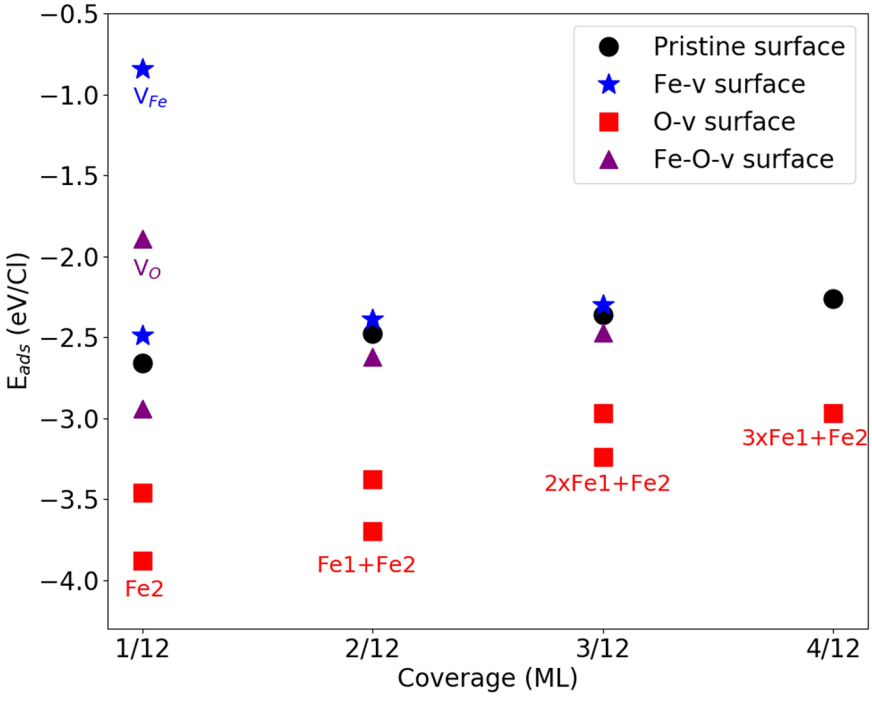

Fig. 5. The Cl adsorption energy on the four surfaces at different Cl coverages. The adsorption on the pristine, Fe-, O- and Fe-O pair vacancy surface are represented with black circles, blue stars, red squares, and purple triangles respectively. The labels below the points are the occupied site(s) if other than Fe1. The number before each site is the number of the site(s) occupied by Cl, e.g. 2 × Fe1 + Fe2 has Cl adsorbed on two Fe1 sites and one Fe2 site.

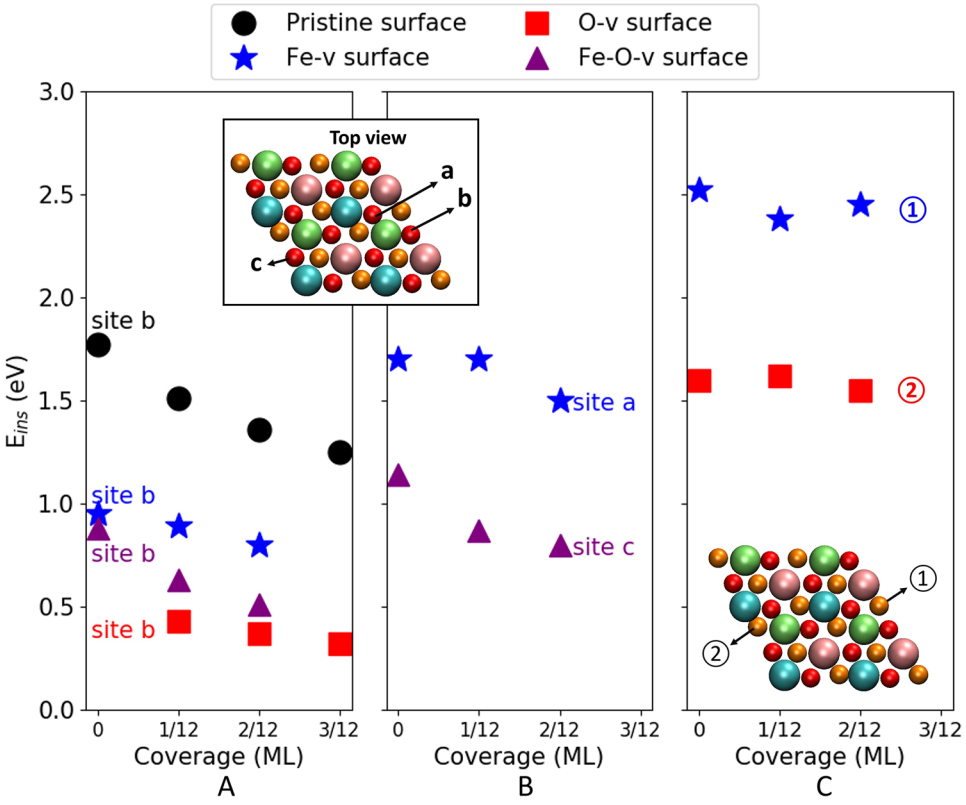

Fig. 6. The insertion energy of Cl into the subsurface. **(A) & (B):** The insertion of Cl from the surface into the second subsurface. The insertion sites are shown on the top view of the pristine surface. **(A)**The insertion into site *b*, which is the site close to the vacancy on the vacancy surfaces. **(B)** The insertion into site *a* and site *c*, which are the sites further away from the vacancies. **(C)** The insertion of Cl from the second layer into the fifth layer for Fe- and O vacancy surfaces. The insertion sites in the fifth layer are labeled as ① and ② respectively and are the closest fifth subsurface sites to the subsurface Cl in figure **A**. The coverages shown here are the Cl coverage on the surface.

decreases slightly with increasing Cl surface coverage, indicating that the insertion becomes less unfavorable with increased coverage of Cl, however, the insertion energy into the fifth subsurface shows no clear dependence on Cl surface coverage. The insertion energy of Cl from the second subsurface into the fifth subsurface (Fig. 6C) is more endothermic than into the second layer (Fig. 6A), indicating that the insertion into deeper subsurface is even less favorable. Subsurface Cl plays a key role in the ion exchange model but here subsurface Cl is found to be less stable than Cl adsorbed on the surface in all cases.

3.4. Surface vacancy formation and stability of vacancies in different layers

To investigate the viability of the point defect model in explaining the Cl-induced depassivation process, the effect of surface Cl and subsurface Cl on the surface Fe- and O vacancy formation is studied. The results are compared with the vacancy formation on the clean pristine surface (Table 2). The stability of Fe- and O vacancy in the bulk relative to the surface is shown in Fig. 7.

The Fe vacancy formation energy on a pristine surface is quite high or about 8.10 eV but the Fe vacancy formation energy decreases by about 18% when Cl is adsorbed on the Fe that later is removed to form the vacancy. Higher Cl coverage has larger effect on the vacancy formation energy (the effect increased by up to 6.3%). On the clean O vacancy surface, the Fe vacancy formation energy is 5.14 eV, which is about 36.5% lower than the clean pristine surface (0 ML Cl coverage) so O vacancy has a larger effect on the Fe vacancy formation than adsorbed Cl. Similar to the pristine surface, the Fe vacancy formation energy decreases with Cl coverage on the O vacancy surface and is 2.56 eV at 3/12 ML, which is 68% less than on the clean pristine surface and 50% less than on the clean O vacancy surface. This indicates that the Cl assists with the formation of surface Fe vacancy. Experimental and theoretical studies have shown that vacancies can exist on the surface of iron oxides [16,18,21–23], and the Cl can lower the formation energy thus increase the Fe vacancy concentration on the surface.

The effect of Cl on the O vacancy formation is also studied on the pristine surface and Fe vacancy surface. On the pristine surface, the formation energy is lowered by up to 45% at Cl coverage of 4/12 ML compared to on the clean pristine surface (6.24 eV). The O vacancy formation energy is 47% lower on the clean Fe vacancy surface compared to on the clean pristine surface and can be further lowered by 16% to 2.77 eV on the Fe vacancy surface at Cl coverage of 3/12 ML. The lowest Fe vacancy formation energy is at higher Cl coverage in presence of O vacancy occupied by Cl while the O vacancy formation becomes comparable to the formation energy of Fe vacancy at higher Cl coverage in the presence of surface Fe vacancy.

The stability of vacancies in the bulk, shown in Fig. 7, is represented as the energy difference of bulk and surface vacancies (Eq. (4)). A positive energy indicates that the vacancy is more stable closer to the surface than deeper in the bulk, while a negative energy suggests that the vacancy is more favorable in the subsurface. For the clean surface, the Fe vacancy is more stable in the bulk while O vacancy is more stable on or close to the surface. The subsurface Fe vacancy becomes more

Table 2
Surface Fe- and O vacancy formation energy on the pristine, O- and Fe vacancy surfaces (Eq. (3)). The coverage (ML) here is the surface coverage of Cl before removing Fe and Cl atoms for Fe vacancy formation.

Surface	Pristine surface					O vacancy surface				Fe vacancy surface			
Coverages (ML)	0/12	1/12	2/12	3/12	4/12	0/12	1/12	2/12	3/12	0/12	1/12	2/12	3/12
Fe vacancy formation energy (eV)	8.10	6.63	6.45	6.26	6.12	5.14	3.23	2.69	2.56	N.A.			
O vacancy formation energy (eV)	6.24	5.01	3.80	3.57	3.43	N.A.				3.28	2.82	2.81	2.77

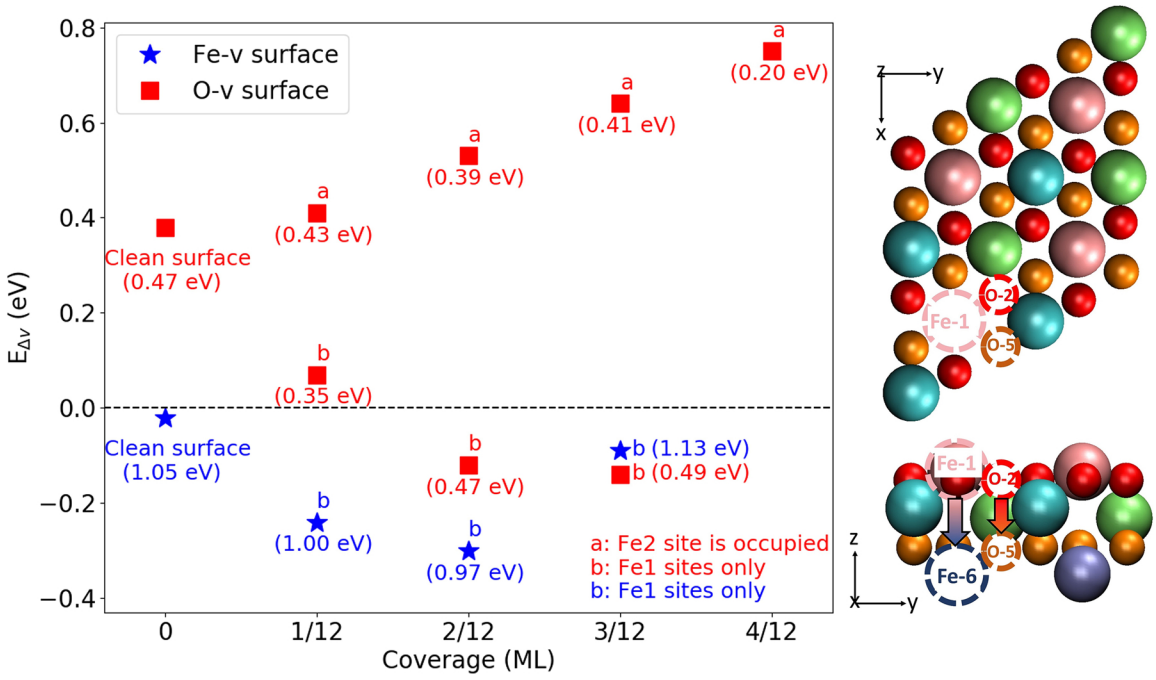

Fig. 7. The energy difference for Fe- and O vacancy in the bulk relative to on the surface (Eq. (4)). For the Fe vacancy surface, the $E_{\Delta v}$ is the energy difference of Fe vacancy in the first (Fe-1) and sixth layer (Fe-6). For the O vacancy surface, the $E_{\Delta v}$ is the energy difference of O vacancy in the second (O-2) and fifth layer (O-5). The calculated diffusion paths for the vacancies are illustrated in the figure inserts. *a* refers to a surface where the Fe2 site is occupied by Cl and *b* to a surface where only the slightly less favorable Fe1 sites are occupied by Cl. A positive energy indicates that the vacancy is energetically more favorable close to the surface while a negative energy indicates more favorable vacancy location in the subsurface. The diffusion barriers (shown in the parentheses) for Fe vacancy and O vacancy are defined as the activation energy for vacancy diffusion toward more favorable positions, that is toward the bulk for Fe vacancy and toward the surface for O vacancy.

favorable with Cl coverage up to 2/12 ML and is slightly less favorable at the highest coverage studied (3/12 ML), but is still more favorable than for the clean surface (0 ML). This indicates that adsorbed Cl helps stabilizing the subsurface Fe vacancy. The Cl coverage has even more effects on the stability of O vacancies in the bulk. When Cl is adsorbed on the most favorable adsorptions site, Fe2, (*a*), the O vacancy becomes more stable close to the surface with higher Cl coverage. However, when Cl is only adsorbed on the Fe1 sites (*b*), which is the slightly less stable adsorption site for Cl (Fig. 5), the energy difference decreases with increasing coverage of Cl and the O vacancy is thermodynamically favored in the bulk at 2/12 ML and 3/12 ML coverage with the energy difference of -0.12 eV and -0.14 eV respectively. However, on the O vacancy surface, the Fe2 site is a more stable adsorption site (about 0.27 – 0.42 eV more stable than Fe1 site) for Cl, suggesting that Fe2 sites are more likely to be occupied by Cl, thus the stability of O vacancy is more likely to be affected by Cl adsorption on the Fe2 site. Overall, the Fe vacancy in the bulk of the oxide is energetically favorable while O vacancy is energetically favorable to be closer to the surface. This is in quantitative agreement with the hypothesis in the point defect model that the Fe vacancy diffuses toward the bulk and O vacancy diffuses toward the surface.

The diffusion barriers for both vacancies are shown in Fig. 7. The diffusion barrier for Fe vacancy is more than twice the diffusion barrier for O vacancy at all coverages. Generally, the Cl coverage has little effect on the diffusion barrier expect on the O vacancy diffusion barrier at high coverage which is half of what at lower coverage.

In a recent paper, Hensley et al. [54] showed that O vacancy stability depends on the effective U value. To verify that our trends stay the same we calculate the stability of the vacancies in the bulk relative to the surface for different values of effective U. The results are shown in Table 3. For this comparison we only consider vacancies at 0 ML Cl coverage, that is without adsorbed Cl on the surface and vary the effective U value from U = 0 to U = 8 eV in increments of 2 eV. The $E_{\Delta v}$ changes with U values for both Fe- and O vacancies, but the relative stability of vacancies remains negative for Fe and positive for O vacancies.

Table 3
The effect of U value on the stability of vacancies in different layers. U = 4 eV is used for all other calculations herein (same as Fig. 7) and listed for comparison.

Effective U value (eV)	Fe vacancy $E_{\Delta v}$ (eV)	O vacancy $E_{\Delta v}$ (eV)
0	−0.44	0.10
2	−0.08	0.19
4	−0.02	0.39
6	−0.16	0.54
8	−0.09	0.56

4. Conclusions

Cl interacts most strongly with the outermost iron sites on the α-Fe_2O_3 surface and is less stable in the subsurface. Cl has stronger interactions with the lower charged Fe atom (Fe^{II}) close to the O vacancies than the Fe^{III} atoms on the surface but the Fe^{II} sites are oxidized to a higher oxidation state upon Cl adsorption. The adsorption energy of Cl increases (less negative) with coverage due to repulsive Cl-Cl interactions on the surface. Higher Cl coverage and surface vacancies make subsurface Cl slightly less unfavorable but never as favorable as surface adsorption making a process where Cl penetrates into the bulk unlikely.

The Fe vacancy formation on the pristine surface and O vacancy surface, with or without Cl in the system, is endothermic. However, Cl can lower the formation energy, indicating that the Cl can assist with the surface Fe vacancy formation. The presence of Cl occupying O vacancy further decreases the formation energy suggesting a mechanism driven by Fe vacancy formation but enhanced by both Cl and O vacancy. Furthermore, the relative stability of Fe- and O vacancies in different layers showed that the Fe vacancies are more stable in the bulk while O vacancies are more stable on the surface. This is consistent with

the vacancy diffusion direction proposed by the point defect model where Fe vacancy diffuses from the oxide/solution interface to the oxide/metal interface and O vacancy diffuses from the oxide/metal interface to the oxide/solution interface.

Overall, our results are in better agreement with the point defect model, and the adsorbed Cl, subsurface Cl and O vacancies may play a role in the surface Fe vacancy formation process, which is one of the key reactions proposed in the point defect model.

Data availability

The raw/processed data required to reproduce these findings cannot be shared at this time as the data also forms part of an ongoing study.

Meanwhile raw/processed data will be made available upon request.

Acknowledgements

This work was supported by the National Science Foundation, DMMI [Grant No. 1435417]. Part of the calculations used the Extreme Science and Engineering Discovery Environment (XSEDE) [55] (TG-ENG170002) which is supported by National Science Foundation grant number ACI-1053575. The authors acknowledge the Texas Advanced Computing Center (TACC) at The University of Texas at Austin and the San Diego Supercomputer Center (SDSC) for providing HPC resources that have contributed to the research results reported within this paper.

Appendix A. Supplementary data

Supplementary data associated with this article can be found, in the online version, at https://doi.org/10.1016/j.corsci.2019.03.052.

References

[1] P. Ghods, O.B. Isgor, F. Bensebaa, D. Kingston, Angle-resolved XPS study of carbon steel passivity and chloride-induced depassivation in simulated concrete pore solution, Corros. Sci. 58 (2012) 159–167.
[2] P. Ghods, O.B. Isgor, J.R. Brown, F. Bensebaa, D. Kingston, XPS depth profiling study on the passive oxide film of carbon steel in saturated calcium hydroxide solution and the effect of chloride on the film properties, Appl. Surf. Sci. 257 (2011) 4669–4677.
[3] H.B. Gunay, P. Ghods, O.B. Isgor, G.J.C. Carpenter, X. Wu, Characterization of atomic structure of oxide films on carbon steel in simulated concrete pore solutions using EELS, Appl. Surf. Sci. 274 (2013) 195–202.
[4] P. Ghods, O.B. Isgor, G.J.C. Carpenter, J. Li, G.A. McRae, G.P. Gu, Nano-scale study of passive films and chloride-induced depassivation of carbon steel rebar in simulated concrete pore solutions using FIB/TEM, Cem. Concr. Res. 47 (2013) 55–68.
[5] H.B. Gunay, O.B. Isgor, P. Ghods, Kinetics of passivation and chloride-induced depassivation of iron in simulated concrete pore solutions using electrochemical quartz crystal nanobalance, Corrosion 71 (2015) 615–627.
[6] M.A. Heine, D.S. Keir, M.J. Pryor, The specific effects of chloride and sulfate ions on oxide covered aluminum, J. Electrochem. Soc. 112 (1965) 24.
[7] D.D. Macdonald, The point defect model for the passive state, J. Electrochem. Soc. 139 (1992) 3434.
[8] M.K. Nieuwoudt, J.D. Comins, I. Cukrowski, Analysis of the composition of the passive film on iron under pitting conditions in 0.05 M NaOH/NaCl using Raman microscopy in situ with anodic polarisation and MCR-ALS, J. Raman Spectrosc. 43 (2012) 928–938.
[9] L.F. Lin, C.Y. Chao, D.D. Macdonald, A point defect model for anodic passive films, J. Electrochem. Soc. 128 (1981) 1194.
[10] C.Y. Chao, L.F. Lin, D.D. Macdonald, A point defect model for anodic passive films, J. Electrochem. Soc. 128 (1981) 1187.
[11] A. Bouzoubaa, B. Diawara, V. Maurice, C. Minot, P. Marcus, Ab initio study of the interaction of chlorides with defect-free hydroxylated NiO surfaces, Corros. Sci. 51 (2009) 941–948.
[12] A. Bouzoubaa, B. Diawara, V. Maurice, C. Minot, P. Marcus, Ab initio modelling of localized corrosion: study of the role of surface steps in the interaction of chlorides with passivated nickel surfaces, Corros. Sci. 51 (2009) 2174–2182.
[13] C.-H. Zhang, M. Liu, Y. Jin, D.-B. Sun, The corrosive influence of chloride ions preference adsorption on α-Al2O3 (0001) surface, Appl. Surf. Sci. 347 (2015) 386–391.
[14] V. Maurice, L.H. Klein, P. Marcus, Atomic structure of metastable pits formed on nickel, Electrochem. Solid-State Lett. 4 (2001) B1.
[15] V. Maurice, L.H. Klein, P. Marcus, Atomic-scale investigation of the localized corrosion of passivated nickel surfaces, Surf. Interface Anal. 34 (2002) 139–143.
[16] R.M. Cornell, U. Schwertmann, The Iron Oxides: Structure, Properties, Reactions, Occurrences and Uses, WILEY-VCH GmbH &Co. KGaA, 2003.
[17] X.G. Wang, W. Weiss, S.K. Shaikhutdinov, M. Ritter, M. Petersen, F. Wagner, R. Schlogl, M. Scheffler, The hematite (alpha-Fe2O3) (0001) surface: evidence for domains of distinct chemistry, Phys. Rev. Lett. 81 (1998) 1038–1041.
[18] M.T. Nguyen, N. Seriani, R. Gebauer, Defective alpha-Fe2O3(0001): an ab initio study, Chemphyschem 15 (2014) 2930–2935.
[19] C.M. Eggleston, A.G. Stack, K.M. Rosso, S.R. Higgins, A.M. Bice, S.W. Boese, R.D. Pribyl, J.J. Nichols, The structure of hematite (α-Fe2O3) (001) surfaces in aqueous media: scanning tunneling microscopy and resonant tunneling calculations of coexisting O and Fe terminations, Geochim. Cosmochim. Acta 67 (2003) 985–1000.
[20] Q. Pang, H. DorMohammadi, O.B. Isgor, L. Arnadottir, Density functional theory study on the effect of OH and Cl adsorption on the surface structure of alpha-Fe2O3, Comput. Theor. Chem. 1100 (2017) 91–101.
[21] L. Ling, J. Song, S. Zhao, R. Zhang, B. Wang, DFT study on the effects of defect and metal-doping on the decomposition of H2S on the α-Fe2O3(0001) surface, RSC Adv. 4 (2014) 22411.
[22] R. Ovcharenko, E. Voloshina, J. Sauer, Water adsorption and O-defect formation on Fe2O3(0001) surfaces, Physical Chem. Chem. Phys. 18 (2016) 25560–25568.
[23] S. Yin, D.E. Ellis, H2O adsorption and dissociation on defective hematite (0001) surfaces: a DFT study, Surf. Sci. 602 (2008) 2047–2054.
[24] P. Hohenberg, W. Kohn, Inhomogeneous Electron gas, Phys. Rev. 136 (1964) B864–B871.
[25] W. Kohn, L.J. Sham, Self-consistent equations including exchange and correlation effects, Phys. Rev. 140 (1965) A1133–A1138.
[26] G. Kresse, J. Furthmuller, Efficient iterative schemes for ab initio total-energy calculations using a plane-wave basis set, Phys. Rev. B 54 (1996) 11169–11186.
[27] G. Kresse, J. Furthmüller, Efficiency of ab-initio total energy calculations for metals and semiconductors using a plane-wave basis set, Comput. Mater. Sci. 6 (1996) 15–50.
[28] G. Kresse, J. Hafner, Ab initio molecular dynamics for liquid metals, Phys. Rev. B 47 (1993) 558–561.
[29] G. Kresse, J. Hafner, Ab initio molecular-dynamics simulation of the liquid-metal–amorphous-semiconductor transition in germanium, Phys. Rev. B 49 (1994) 14251–14269.
[30] P.E. Blöchl, Projector augmented-wave method, Phys. Rev. B 50 (1994) 17953–17979.
[31] J.P. Perdew, K. Burke, M. Ernzerhof, Generalized gradient approximation made simple, Phys. Rev. Lett. 77 (1996) 3865–3868.
[32] J.P. Perdew, K. Burke, M. Ernzerhof, Generalized gradient approximation made simple, Phys. Rev. Lett. 77 (1996) 3865 ERRATA, Phys. Rev. Lett., 78 (1997) 1396-1396.
[33] V.I. Anisimov, J. Zaanen, O.K. Andersen, Band theory and Mott insulators: Hubbard U instead of Stoner I, Phys. Rev. B 44 (1991) 943–954.
[34] M. Cococcioni, S. de Gironcoli, Linear response approach to the calculation of the effective interaction parameters in the LDA + Umethod, Phys. Rev. B (2005) 71.
[35] A.I. Liechtenstein, V.I. Anisimov, J. Zaanen, Density-functional theory and strong interactions: orbital ordering in Mott-Hubbard insulators, Phys. Rev. B 52 (1995) R5467–R5470.
[36] I.V. Solovyev, P.H. Dederichs, V.I. Anisimov, Corrected atomic limit in the local-density approximation and the electronic structure of d impurities in Rb, Phys. Rev. B 50 (1994) 16861–16871.
[37] V.I. Anisimov, F. Aryasetiawan, A.I. Lichtenstein, First-principles calculations of the electronic structure and spectra of strongly correlated systems: the LDA + U method, J. Phys. Condens. Matter 9 (1997) 767–808.
[38] S.L. Dudarev, G.A. Botton, S.Y. Savrasov, C.J. Humphreys, A.P. Sutton, Electron-energy-loss spectra and the structural stability of nickel oxide: an LSDA + U study, Phys. Rev. B 57 (1998) 1505–1509.
[39] H.J. Monkhorst, J.D. Pack, Special points for Brillouin-zone integrations, Phys. Rev. B 13 (1976) 5188–5192.
[40] M. Yu, D.R. Trinkle, Accurate and efficient algorithm for Bader charge integration, J. Chem. Phys. 134 (2011) 064111.
[41] W. Tang, E. Sanville, G. Henkelman, A grid-based Bader analysis algorithm without lattice bias, J. Phys. Condens. Matter 21 (2009) 084204.
[42] E. Sanville, S.D. Kenny, R. Smith, G. Henkelman, Improved grid-based algorithm for Bader charge allocation, J. Comput. Chem. 28 (2007) 899–908.
[43] G. Henkelman, A. Arnaldsson, H. Jónsson, A fast and robust algorithm for Bader decomposition of charge density, Comput. Mater. Sci. 36 (2006) 354–360.
[44] G. Henkelman, B.P. Uberuaga, H. Jónsson, A climbing image nudged elastic band method for finding saddle points and minimum energy paths, J. Chem. Phys. 113 (2000) 9901–9904.
[45] L.W. Finger, R.M. Hazen, Crystal structure and isothermal compression of Fe2O3, Cr2O3, and V2O3 to 50 kbars, J. Appl. Phys. 51 (1980) 5362.
[46] O. Neufeld, M.C. Toroker, Platinum-doped α-Fe2O3 for enhanced water splitting efficiency: a DFT + U study, J. Phys. Chem. C 119 (2015) 5836–5847.
[47] J.Y.T. Chan, S.Y. Ang, E.Y. Ye, M. Sullivan, J. Zhang, M. Lin, Heterogeneous photo-Fenton reaction on hematite (alpha-Fe2O3){104}, {113} and {001} surface facets, Phys. Chem. Chem. Phys. 17 (2015) 25333–25341.
[48] F. Ciccacci, L. Braicovich, E. Puppin, E. Vescovo, Empty electron states in Fe2O3 by ultraviolet inverse-photoemission spectroscopy, Phys. Rev. B 44 (1991) 10444–10448.
[49] A. Fujimori, M. Saeki, N. Kimizuka, M. Taniguchi, S. Suga, Photoemission satellites and electronic structure of Fe2O3, Phys. Rev. B 34 (1986) 7318–7328.
[50] T. Uozumi, K. Okada, A. Kotani, Theory of photoemission spectra for M2O3(M = Ti, V, Cr, Mn, Fe) compounds, J. Electron Spectros. Relat. Phenomena 78 (1996) 103–106.
[51] J. Lee, S. Han, Thermodynamics of native point defects in alpha-Fe2O3: an ab initio study, Phys. Chem. Chem. Phys. 15 (2013) 18906–18914.
[52] T.J. Smart, Y. Ping, Effect of defects on the small polaron formation and transport properties of hematite from first-principles calculations, J. Phys. Condens. Matter 29 (2017) 394006.

[53] E. Krén, P. Szabó, G. Konczos, Neutron diffraction studies on the (1 − x) Fe2O3 − xRh2O3 system, Phys. Lett. 19 (1965) 103–104.
[54] A.J.R. Hensley, Y. Wang, J.-S. McEwen, The partial reduction of clean and doped α-Fe2O3(0001) from first principles, Appl. Catal. A Gen. (2019).
[55] J. Towns, T. Cockerill, M. Dahan, I. Foster, K. Gaither, A. Grimshaw, V. Hazlewood, S. Lathrop, D. Lifka, G.D. Peterson, R. Roskies, J.R. Scott, N. Wilkens-Diehr, XSEDE: accelerating scientific discovery, Comput. Sci. Eng. 16 (2014) 62–74.